

Controllable Hydrothermal Synthesis of Spinel LiMn_2O_4 and its Electrochemical Properties

X.D. Luo^{1,‡}, W. Zeng¹, M. Yuan¹, B. Huang^{1,2}, Y.W. Li^{1,2}, J.W. Yang^{1,2}, S.H. Xiao^{1,2,*}

¹ Guangxi Key Laboratory of Electrochemical and Magneto-chemical Functional Materials, College of Chemistry and Bioengineering, Guilin University of Technology, Guilin 541004, China

² Guilin University of Technology, Collaborative Innovation Center for Exploration of Hidden Nonferrous Metal Deposits and Development of New Materials in Guangxi, Guilin University of Technology, Guilin 541004, China

*E-mail: 420466855@qq.com

Received: 10 April 2018 / Accepted: 25 May 2018 / Published: 5 July 2018

Using MnO_2 as manganese source, and $\text{LiOH}\cdot\text{H}_2\text{O}$ as lithium source, spinel LiMn_2O_4 with excellent electrochemical performances was synthesized by changing hydrothermal time, hydrothermal temperature and annealing temperature. The phase and microstructure were investigated by X-ray diffraction (XRD) measurement, scanning electron microscope (SEM), and the electrochemical performances were studied by electrochemical workstation. The results indicated LiMn_2O_4 powder was well-dispersed rod-like particle, the average particle size was 100 nm or so, which delivered a high first discharge capacity of $128 \text{ mAh}\cdot\text{g}^{-1}$ and $126 \text{ mAh}\cdot\text{g}^{-1}$ at 0.2 C and 0.5 C respectively, remaining $110 \text{ mAh}\cdot\text{g}^{-1}$ after 100 charge-discharge cycles at 0.5 C.

Keywords: Hydrothermal method; Spinel LiMn_2O_4 ; electrochemical performance; improved synthesis methods

1. INTRODUCTION

The theoretical specific capacity of spinel structure lithium manganese oxides was $148 \text{ mAh}\cdot\text{g}^{-1}$. Compared to lithium manganese oxide in the layered structure, the typical three-dimensional space tunnel structure was more favorable for Li^+ in the $[\text{Mn}_2\text{O}_4]$ three-dimensional channel reversible insertion/extraction, and therefore showed excellent electrochemical performance [1-4]. Due to so many advantages, such as rich raw materials, good safety performance, clean environmental protection, high discharge voltage, spinel LiMn_2O_4 had been demonstrated as one of the hot spots in the lithium-ion battery research [5-10]. However, the spinel-type lithium manganese oxide materials are prone to Jahn-Teller distortion effect, active substance manganese in the electrolyte slowly

dissolved and the decomposition of electrolyte during the charge and discharge process, which seriously affected its cycling performance [11-17]. In order to improve the capacity of the spinel-type lithium manganese oxide cathode materials, the improved synthesis methods, ion doping and surface coating were generally adopted to stabilize its spinel-type structure, thereby enhancing the electrochemical properties of the materials to a certain extent [18-23].

By controlling different hydrothermal temperatures and times, a lithium manganese oxide cathode material with rod-like morphology and nano-size was synthesized. This structure of lithium manganese oxide could effectively shorten the diffusion path of lithium ions and improve the diffusion rate of lithium ions, as well as improve the tap density [24], and then increase its energy density [25]. In this paper, the lithium manganese oxide cathode materials with excellent electrochemical performances were successfully synthesized.

2. EXPERIMENTAL

2.1 Synthesis of MnO_2 Precursors

$MnSO_4 \cdot H_2O$ and $Na_2S_2O_8$ as raw materials, and dissolved in a beaker according to a certain stoichiometric ratio with a certain amount of distilled water, stirring with a thermostatic magnetic stirrer until the mixture completely dissolved. The dissolved mixed solution was put into a 100 mL Teflon-lined stainless steel autoclave at different temperatures of 80 °C, 100 °C, 120 °C for 10 h and at different times of 8 h, 10 h, 12 h for 100 °C, and cooled to room temperature. After filtration, and then washed with deionized water and anhydrous ethanol several times. The washed black precipitate was dried in an oven at 80 °C for 20 h or longer to obtain MnO_2 precursors.

2.2 Synthesis of spinel lithium manganite

Based on the prepared MnO_2 , $LiOH \cdot H_2O$ was added according to a certain proportion, mixed and scattered with absolute ethanol, then dried in a blast oven at 80 °C for a period of time. The dried samples were ground in agate mortar with an appropriate amount of ethanol, and the samples were pre-sintered at 450 °C for 6 h in the muffle furnace, then the temperature was raised to 750 °C for 18 h with a heating rate of 5 °C \cdot min⁻¹. After natural cooling to room temperature, the required spinel $LiMn_2O_4$ samples were obtained.

2.3. Structural characterization

The crystal structure of the powders was characterized with X-ray diffraction (XRD) measurement (Panalytical X'Pert PRO MRD, Holland) with a Cu K α radiation operated at 40 kV and 40 mA. The scanning step was 0.02626°, the scanning speed was 0.6565°/s and the range was 10-80°. The morphology of the samples was evaluated by field emission scanning electron microscopy (FE-SEM SU5000).

2.4. Electrochemical measurement

Using the synthesized spinel lithium manganese oxide cathode materials as the active material, the mixtures of the active materials: poly (vinyl difluoride) PVDF: carbon black = 8: 1: 1 (mass ratio) in N-methyl-2-pyrrolidone solvent were coated on aluminum foil, the surface area of electrode material was 1.766 cm², the average weight of active material was 1.68 mg. Metallic lithium foil was used as the negative electrode. The electrolyte was 1M LiPF₆ solution in ethylene carbonate (EC) and dimethyl carbonate (DMC) (volume ration of 1: 1). Celgard 2300 polyethylene film was used as the separator. In the relative water standard less than 0.1 ppm, oxygen standard less than 0.1 ppm high purity argon glove box for the type of CR2016 coin cells assembly. Electrochemical impedance spectra (EIS) was performed on an electrochemical working station under room temperature conditions (Init E(V)=2.98, High frequency(Hz)= 1×10⁵, Low frequency(Hz)= 0.1, CHI760e, Shanghai Chenhua Co., Ltd., China). Electrochemical impedance fitting was carried out with Zview software. Charge/discharge tests and rate test were performed using the NEWARE batteries test system (BTS-4000, Shenzhen New will Co., Ltd., China) with different current densities.

3. RESULTS AND DISCUSSION

3.1 Hydrothermal temperature

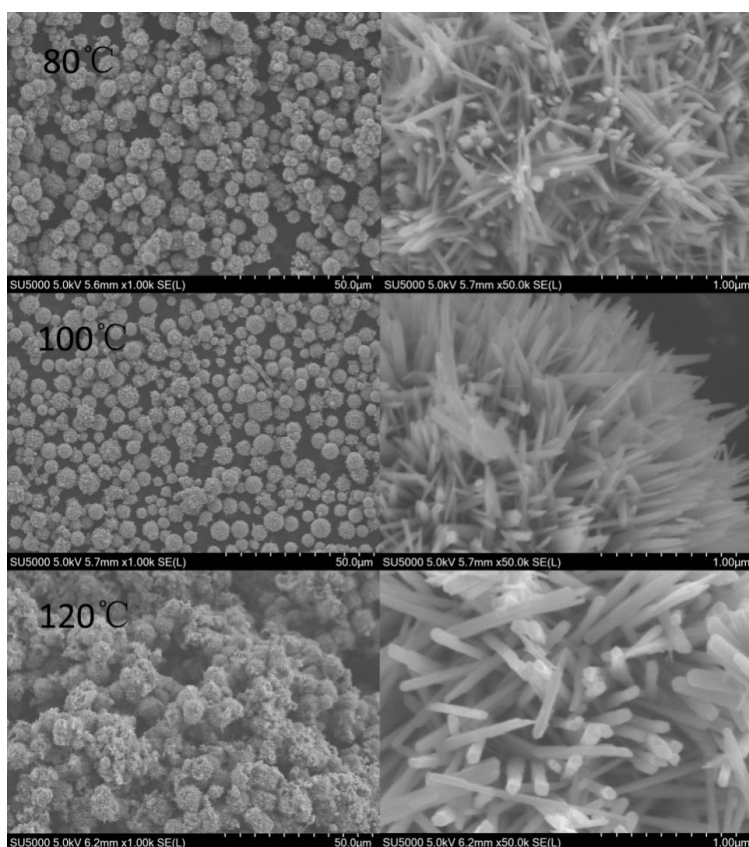


Figure 1. SEM images of MnO₂ precursors synthesized at 80 °C, 100 °C and 120 °C for 10 h

Figure 1 were the SEM images of the manganese dioxide precursors synthesized at different hydrothermal temperatures (80 °C, 100 °C, 120 °C) for 10 h. Seen from the figure, the manganese dioxide precursors were spherical particles accumulated by a large number of nanometer rodlike crystal. When the hydrothermal reaction temperature was at 100 °C, the diameter of nanorod was the smallest, about 30-40 nm, and the spherical particles had better dispersibility and lower aggregation. Compared with the 100 °C sample, the dispersion and uniformity of the 80 °C sample was poor. When the temperature was raised to 120 °C, the particles size increased, and the spherical morphology of the particles was gradually destroyed and had a more pronounced reunion.

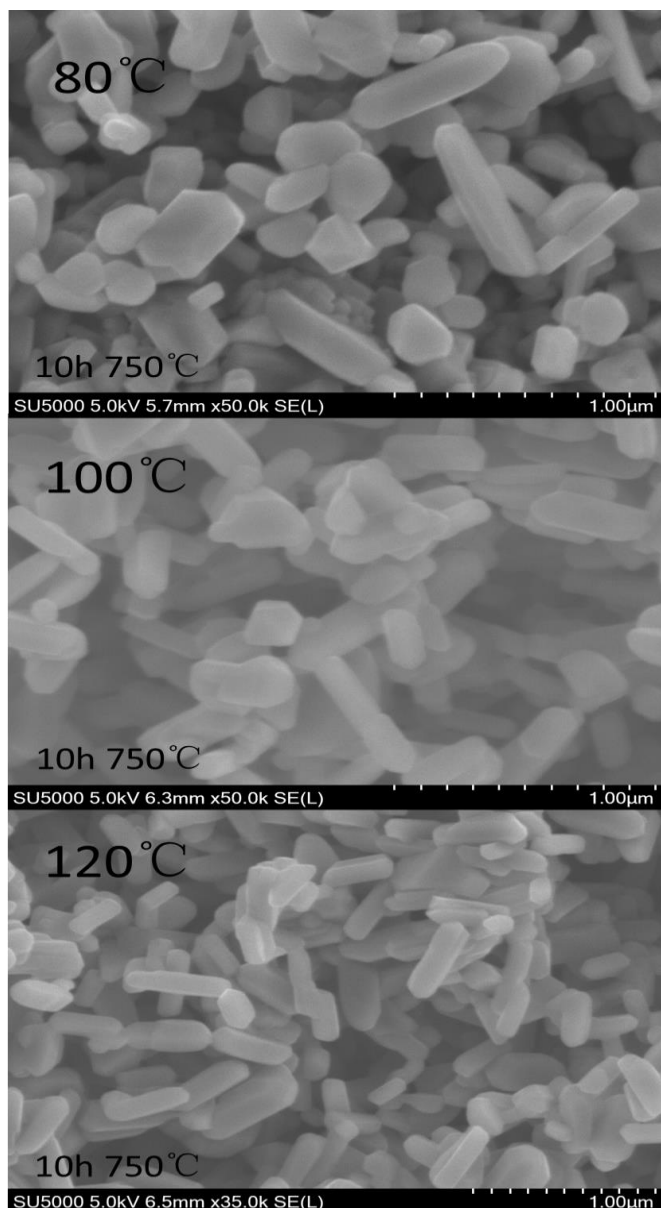


Figure 2. SEM images of LiMn_2O_4 samples synthesized at different hydrothermal temperatures of 80 °C, 100 °C and 120 °C for 10 h, sintering at 750 °C

Figure 2 were the particles size and morphology pictures of LiMn_2O_4 samples by using manganese dioxide as precursors synthesized at different hydrothermal temperatures. It could be seen

that all the samples were nanorods or spherical morphology, and the diameter of particles was between 100 and 200 nm. In comparison, the lithium manganese oxide sample synthesized at 100 °C had smaller spherical particles and better dispersion than those of other samples, which helped to improve the tap density of the materials along with higher energy density. With the increase of hydrothermal temperature, the spherical particles gradually decreased, and the rod-shaped particles gradually increased, along with a certain degree of reunion. This may be ascribed to the following reasons that high temperature could result in the disorderly accumulation of manganese dioxide precursors, and formed the uneven lithium manganese oxide particles.

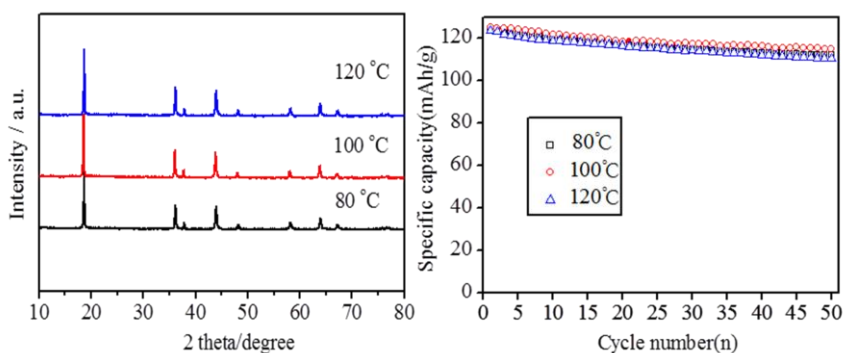


Figure 3. (a) XRD patterns (b) cycle performance of LiMn_2O_4 samples synthesized at 80 °C, 100 °C and 120 °C, respectively

The XRD patterns of LiMn_2O_4 by using manganese dioxide as precursors synthesized at different hydrothermal temperatures were illustrated in Figure 3 (a). Obviously, no impurity peaks were found in the XRD diagrams, which exactly corresponded to the standard card (JCPDS card no.35-0782). The sharp and relatively high diffraction peaks indicated that the synthesized materials had higher purity and better crystallinity, as described in the literature [26].

Figure 3 (b) were the cycle performance profiles of the lithium manganese oxide samples synthesized at different hydrothermal temperatures at 0.5 C. The discharge specific capacity and corresponding capacity retention ratio after 50 charge/discharge cycles were displayed in Table 1.

Table 1. The discharge capacity in different cycling number and corresponding retention rates of samples

Sample	Temperature (°C)	1 st Discharge Capacity ($\text{mAh}\cdot\text{g}^{-1}$)	50 th Discharge Capacity ($\text{mAh}\cdot\text{g}^{-1}$)	Capacity Retention Ratio
LiMn_2O_4	80	124	112	90
	100	125	115	91.9
	120	123	111	89.8

From the table, the hydrothermal temperature had a certain impact on the charge and discharge properties of the lithium manganese oxide materials. Due to relatively smaller particles at hydrothermal temperature of 100 °C, which improved the effective contact area between materials and electrolyte, shortened the diffusion path of lithium ions, made conduction rate of lithium ions faster, and then improved discharge specific capacity. At the current density of 0.5 C, the first discharge specific capacities of the lithium manganese oxide materials corresponding to 80 °C, 100 °C and 120 °C were 124 mAh·g⁻¹, 125 mAh·g⁻¹ and 123 mAh·g⁻¹, which were respectively corresponding to 112 mAh·g⁻¹, 115 mAh·g⁻¹ and 111 mAh·g⁻¹ after 50 cycles. The cycle performance of the lithium manganese oxide sample under 100 °C hydrothermal temperature was best than that of the other two samples, and its capacity retention rate was also highest and reached to 91.9%.

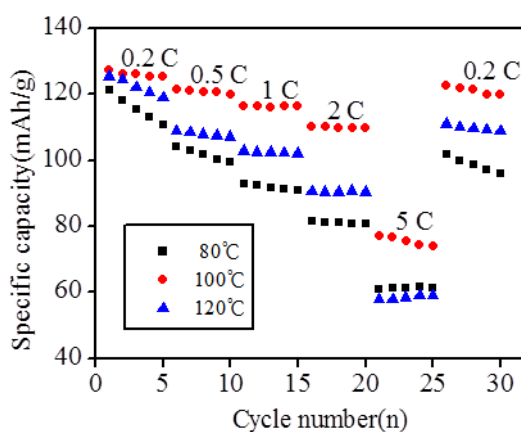


Figure 4. Rate profiles of the samples synthesized at 80 °C, 100 °C and 120 °C

The rate capabilities of the samples synthesized at different hydrothermal temperatures were showed in Figure 4. It can be seen from the figures, the capacity attenuation of three materials in the low rate discharge was not more obvious, but the attenuation amplitude varied greatly under high rate charge and discharge. After a series of high rate charge-discharge cycles, the discharge capacity for the sample synthesized at 100 °C can be maintained 120 mAh·g⁻¹ at 0.2 C, enjoying 94.7% capacity retention ratio, higher than the 83.2% and 88.6% capacity retention ratio for the other samples, which exhibited that the material synthesized at 100 °C had excellent rate capability, such as the good capacity retention ratio and reversibility.

3.2 Hydrothermal time

Figure 5 were the SEM images of MnO₂ synthesized at 100 °C for different hydrothermal times (8 h, 10 h, 12 h). We can see that the manganese dioxide precursors using the manganese sulfate monohydrate and sodium persulfate as raw materials were the sea urchin spherical particles composed of nanorods.

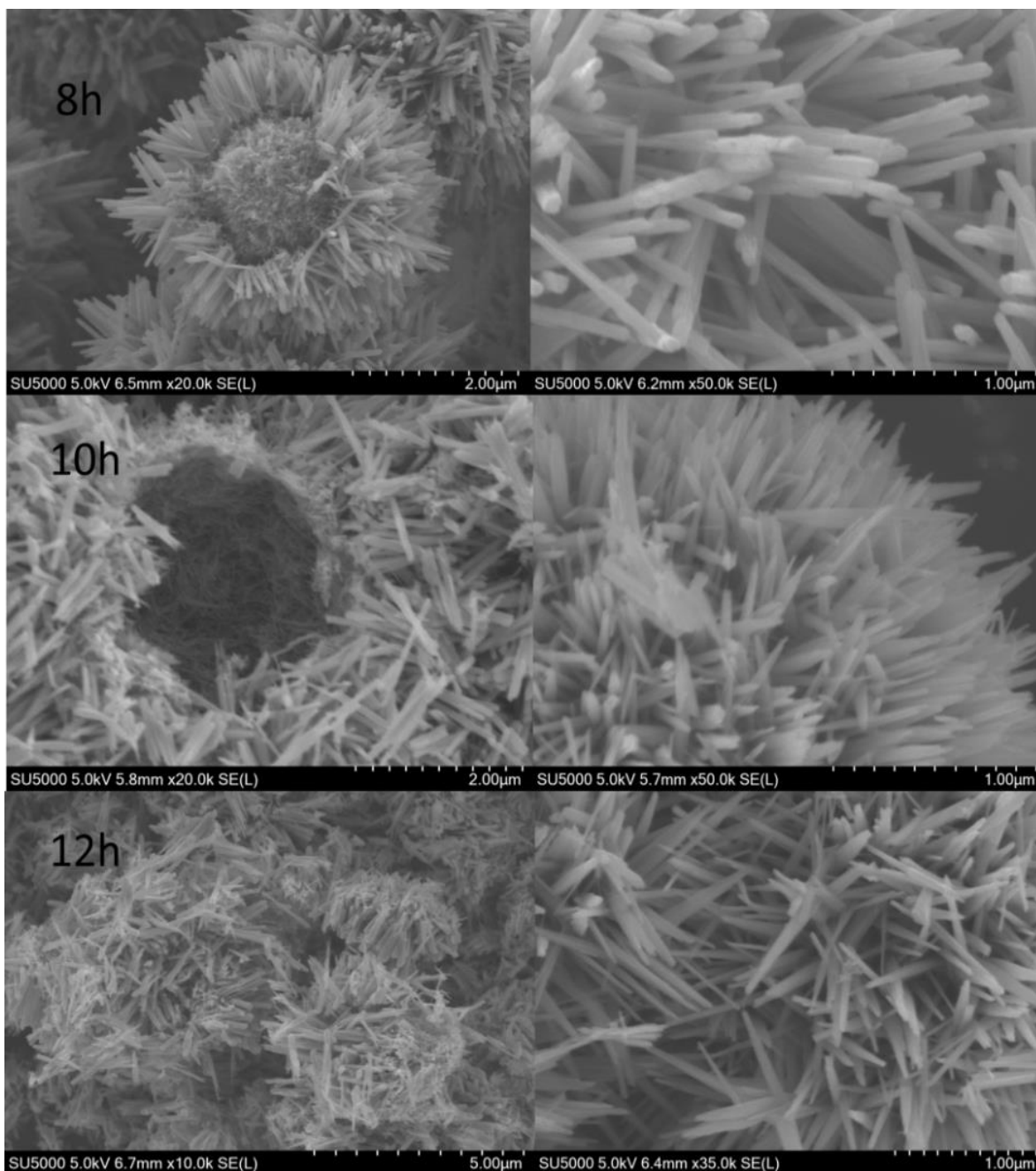


Figure 5. SEM images of MnO₂ synthesized at 100 °C for 8 h, 10 h and 12 h

When the hydrothermal reaction time was 8 h, the particles size of the material with a core-shell structure was about 4 µm. When the reaction time was increased to 10 h, the nanorods were packed in order and arranged closely, the central nucleus disappeared and hollow spheres were formed. This was reported to have a positive impact on electrochemical performance of synthesized electrode materials [27]. With the increase of reaction time, the length of nanorods had no obvious change, but the spherical morphology composed of nanorods was gradually destroyed, and the hollow spherical structure disappeared.

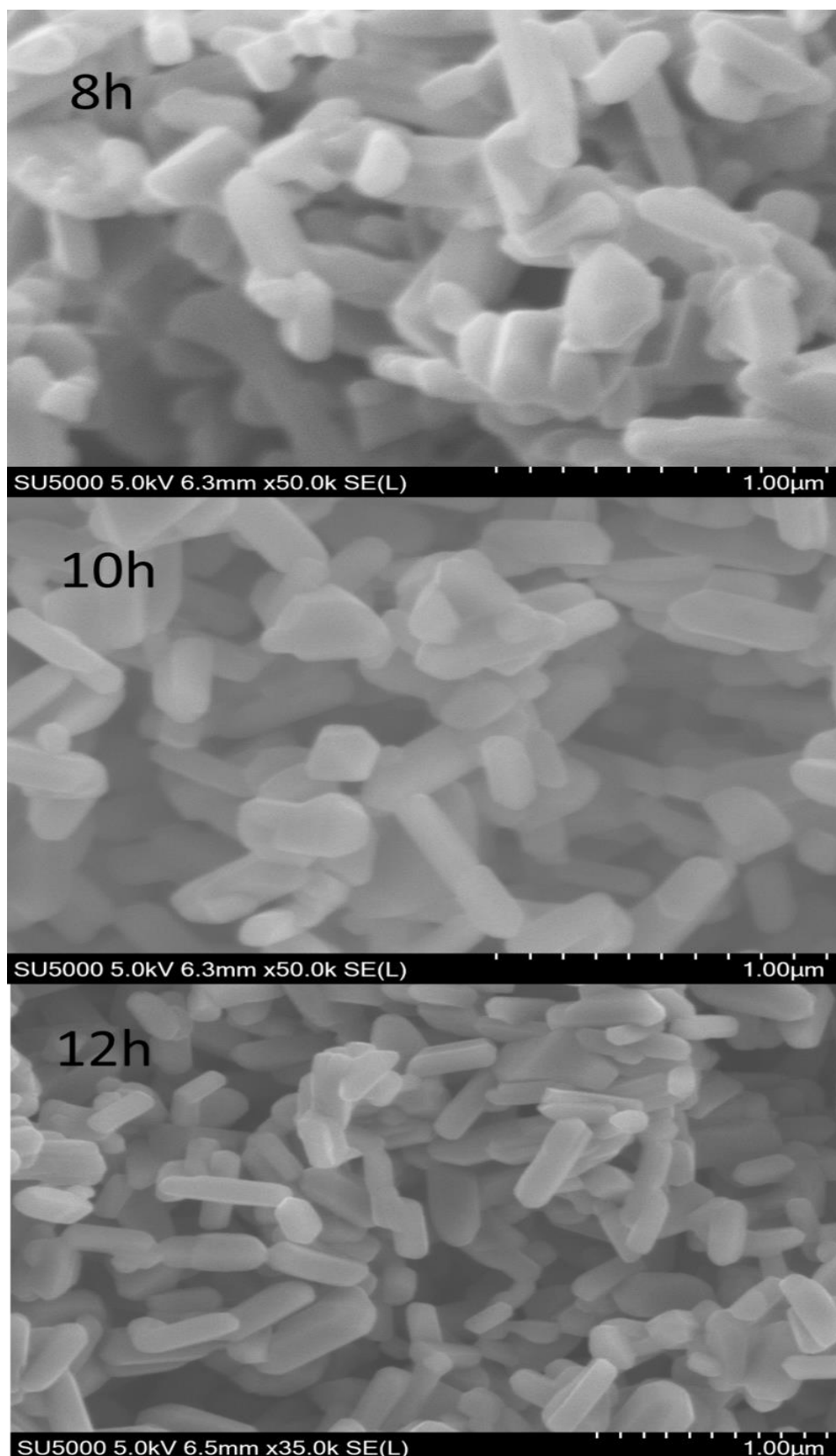


Figure 6. SEM images of LiMn_2O_4 at $100\text{ }^\circ\text{C}$ for 8 h, 10 h and 12 h, sintering at $750\text{ }^\circ\text{C}$

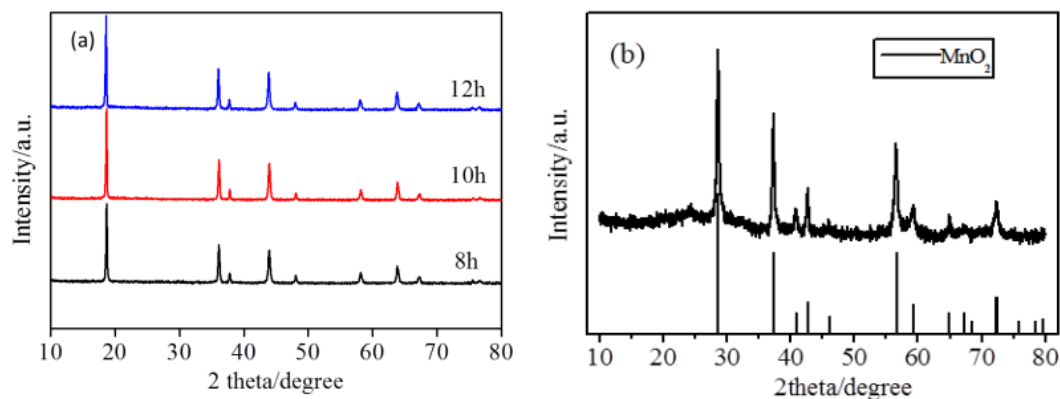


Figure 7. XRD patterns of (a) LiMn_2O_4 synthesized at $100\text{ }^\circ\text{C}$ for 8 h, 10 h and 12 h (b) MnO_2 precursor under $100\text{ }^\circ\text{C}$ for 10 h

Figure 6 were the SEM images of LiMn_2O_4 synthesized from MnO_2 precursors formed at different hydrothermal times. It can be seen that the LiMn_2O_4 particles were rod-shaped and spherical morphology with good dispersivity, as well as smooth and regular surface. And with the extension of the reaction time, the particles size showed a trend of increasing gradually. Research shows that smaller particle size is beneficial to increasing the diffusion rate of lithium ions [28-29].

Figure 7 (a) showed the XRD patterns of LiMn_2O_4 samples synthesized from MnO_2 precursors synthesized at different hydrothermal times. The diffraction peaks of the samples corresponded to the spinel LiMn_2O_4 standard card, which indicated that the synthesized samples had a cubic spinel structure. And with the extension of the hydrothermal time, the characteristic peaks of the samples became sharper and sharper, which meant that the degree of crystallization was increasing and the grains size was becoming larger and larger. The XRD pattern of MnO_2 precursor at $100\text{ }^\circ\text{C}$ for 10 h was exhibited in Figure 7 (b), there was no other impure peak could be found and the peaks were sharp, indicating the degree of crystallization was well, which would certainly have a positive effect on crystallinity, morphology and electrochemical properties of resulting LiMn_2O_4 samples.

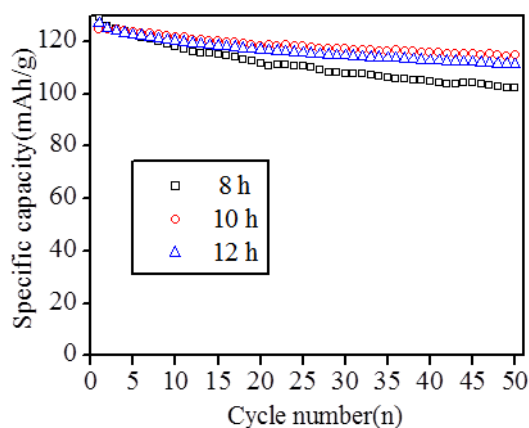


Figure 8. Cycle performance of LiMn_2O_4 synthesized at $100\text{ }^\circ\text{C}$ for 8 h, 10 h and 12 h, sintering at $750\text{ }^\circ\text{C}$

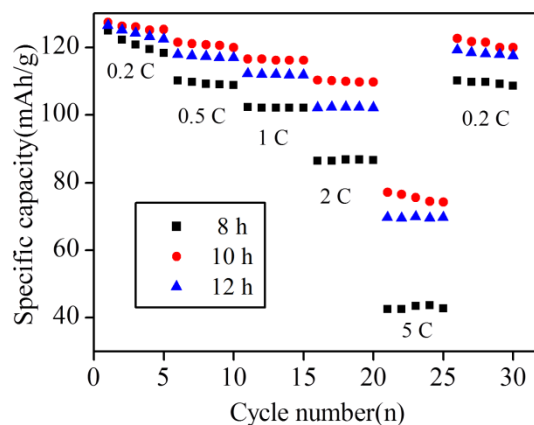


Figure 9. Rate performance of LiMn_2O_4 synthesized at $100\text{ }^\circ\text{C}$ for 8 h, 10 h and 12 h, sintering at $750\text{ }^\circ\text{C}$.

Figure 8 were the cycle performance diagrams of three samples synthesized at hydrothermal times of 8 h, 10 h, and 12 h at the rate of 0.5 C. The first discharge specific capacities of the three samples were $129\text{ mAh}\cdot\text{g}^{-1}$, $126\text{ mAh}\cdot\text{g}^{-1}$, $127\text{ mAh}\cdot\text{g}^{-1}$, respectively. After 50 charge and discharge cycles, the corresponding discharge specific capacities were $102\text{ mAh}\cdot\text{g}^{-1}$, $115\text{ mAh}\cdot\text{g}^{-1}$, $111\text{ mAh}\cdot\text{g}^{-1}$, and the capacity retention ratio were 79.2%, 91.2% and 87.6%, respectively. The results showed that the materials had higher initial discharge capacities at 8 h and 12 h, but their capacities decayed faster. By comparison, the material synthesized for 10 h hydrothermal time had the best cycle performance and the highest capacity retention ratio.

Figure 9 showed the rate properties of various materials synthesized at different hydrothermal times. It can be seen from the figure, with the increase of charge-discharge rate, the discharge specific capacity was continuously decreasing [30]. By comparison, the attenuation of the sample synthesized for 10 h hydrothermal time was less affected by increasing charge-discharge rate. After from 0.2 C to 5 C rate cycles, and then back to 0.2 C rate discharge, the discharge specific capacity of three samples were $109\text{ mAh}\cdot\text{g}^{-1}$, $120\text{ mAh}\cdot\text{g}^{-1}$ and $117\text{ mAh}\cdot\text{g}^{-1}$ corresponding to 8 h, 10 h, 12 h hydrothermal reaction condition, respectively, and theirs corresponding capacity retention ratios were 86.3%, 93.5%, 92.3%. It was obvious that the capacity retention ratio and reversibility of the sample obtained by 10 h hydrothermal reaction time was relatively better.

3.3 Sintering temperature.

Based on the previous optimized hydrothermal reaction conditions, the precursors of manganese dioxide had been prepared by controlling the hydrothermal temperature of $100\text{ }^\circ\text{C}$ and reaction time of 10 h. Then the effects of different sintering temperatures ($700\text{ }^\circ\text{C}$, $750\text{ }^\circ\text{C}$, $800\text{ }^\circ\text{C}$) on the structure and electrochemical properties of lithium manganese oxide cathode materials had been investigated.

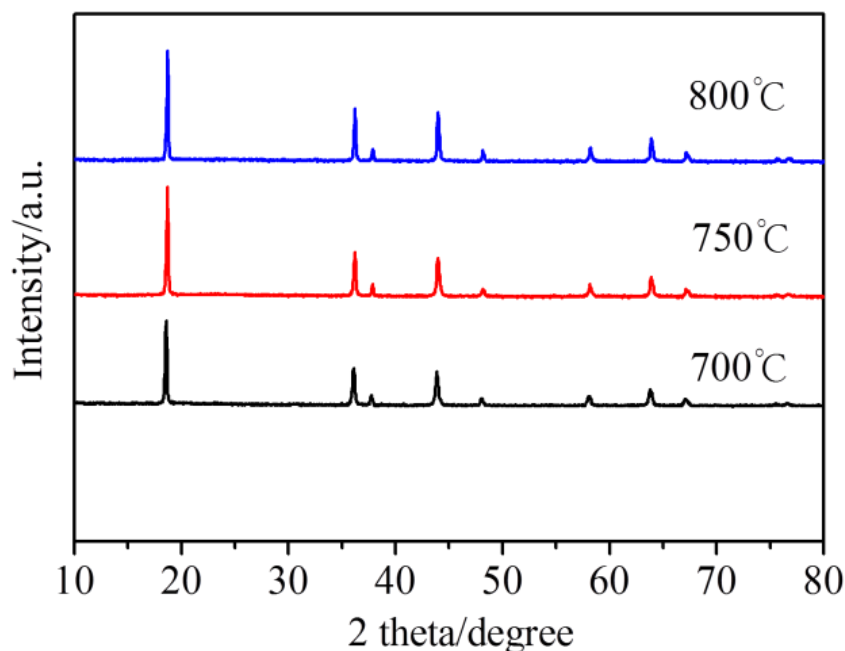


Figure 10. XRD patterns of LiMn_2O_4 samples synthesized at 700 °C, 750 °C and 800 °C.

Figure 10 were the XRD patterns of LiMn_2O_4 materials prepared at different sintering temperatures (700 °C, 750 °C, 800 °C). It is not difficult to find that the diffraction peaks of the samples corresponded to the spinel LiMn_2O_4 standard card, there were no other impurity peaks, which indicated that the spinel LiMn_2O_4 materials synthesized by manganese dioxide precursors and lithium source mixture via different sintering temperatures had very high purity. The high and sharp diffraction peaks showed that the crystallinity of the samples were ideal.

The SEM images of samples sintered at three different temperatures were displayed in Figure 11. It was that can be seen, the resulting product was almost all rod-like particles at the sintering temperature of 700 °C, the shape and size of the particles was uneven, and their diameter was about 100-200 nm. The rodlike particles may be resulted from the abscission and transformation of the outer layer needle structure of the precursors MnO_2 . When the sintering temperature reached to 750 °C, nanorods gradually became shorter and thicker, and then began to change to nano-spherical particles. Only a few of the particles retained the original rodlike structure, and most of them were about 150 nm. With the continuous increase of temperature, nano-rod-like particles had completely changed into the nano-spherical particles, the surface of the particles was smooth and the crystallization was perfect, but accompanied by serious agglomeration. Therefore, the sintering temperature not only influenced the crystal shape and purity of the samples, but also had an important influence on the morphology of the products.

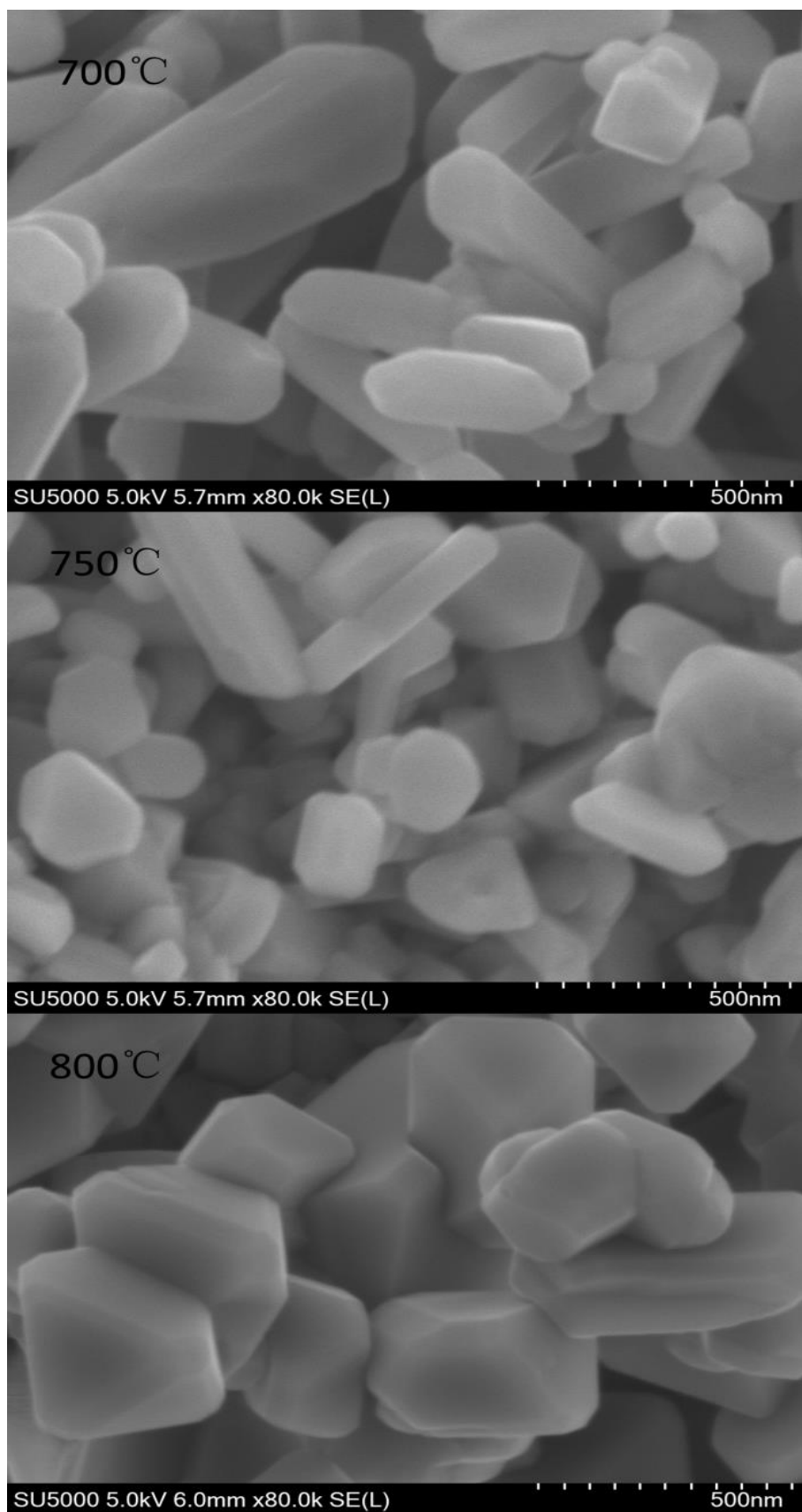


Figure 11. SEM images of LiMn_2O_4 synthesized at 700 °C, 750 °C and 800 °C.

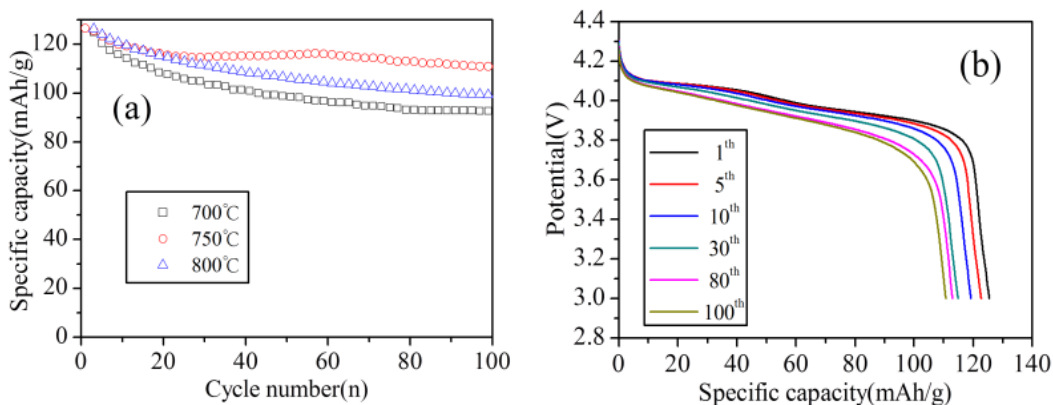


Figure 12. (a) Cycle performance of three electrode materials synthesized at 700 °C, 750 °C and 800 °C, (b) charge/discharge curves of the resulting LiMn_2O_4 sample at 750 °C.

Figure 12 (a) showed the cycle performance of the materials obtained at different sintering temperatures at 0.5 C. It can be found that the initial discharge capacity of the sample obtained at 750 °C was $126 \text{ mAh}\cdot\text{g}^{-1}$, after 100 charge-discharge cycles, the discharge capacity was still maintained at $110 \text{ mAh}\cdot\text{g}^{-1}$, the capacity retention ratio was up to 87.3%. By comparison, the initial discharge specific capacities of the samples sintered at 700 °C and 800 °C were $130 \text{ mAh}\cdot\text{g}^{-1}$ and $125 \text{ mAh}\cdot\text{g}^{-1}$, respectively. The corresponding discharge capacity decreased to $92.4 \text{ mAh}\cdot\text{g}^{-1}$ and $101.5 \text{ mAh}\cdot\text{g}^{-1}$ after 100 charge and discharge cycles, and the capacity retention ratios were only 71.1% and 81.2%. Thus, when the sintering temperature was too high or too low, although the initial discharge capacity were well, the capacity retention ratios were relatively low, and the cycle performance were poor. It may be explained as follows: for the sample sintered at 700 °C, the relative poor crystallinity was the main factor affecting the cycle performance, and for the sample sintered at 800 °C, although it had been completely crystalline, there was still serious reunion, as well as some structure damages, which resulted in poor cycle performance. The charge/discharge curve of the obtained LiMn_2O_4 positive electrode for 750 °C was displayed in Figure 12 (b). We could see that the insertion/extraction potentials of lithium ion was constantly shortening and reducing with the increase of charge and discharge cycles. This was due to that the crystal structure of the material was destroyed during lithium ions embed and prolapsed from lattices, resulting in enlarging polarization and decreasing capacity.

In order to have a comparison on the rate properties of several different materials, these materials were tested at different rates (0.2 C, 0.5 C, 1 C, 2 C, 5 C and 10 C) for charge and discharge cycles, and the discharge specific capacities data were shown in Figure 13. The initial discharge specific capacities of the samples sintered at 750 °C were $128 \text{ mAh}\cdot\text{g}^{-1}$, $124 \text{ mAh}\cdot\text{g}^{-1}$, $118 \text{ mAh}\cdot\text{g}^{-1}$, $116 \text{ mAh}\cdot\text{g}^{-1}$, $84 \text{ mAh}\cdot\text{g}^{-1}$, $22 \text{ mAh}\cdot\text{g}^{-1}$, respectively, corresponding to the rate of 0.2 C, 0.5 C, 1 C, 2 C, 5 C and 10 C. Therefore, within 5 C, the capacity sill remained $80 \text{ mAh}\cdot\text{g}^{-1}$ after several charge and discharge cycles, indicating that the sample sintered at 750 °C had relatively ideal capacity retention ratio and rate capability. In addition, we could see that the discharge specific capacity for the 750 °C-sintered LiMn_2O_4 sample electrode drastically decreased compared with the other electrodes at high

rates, this may be due to the fact that lithium ions diffusion rate and electrons transfer rate can't meet the requirements of high rates and performed more obvious than the others, resulting in the most increase of polarization.

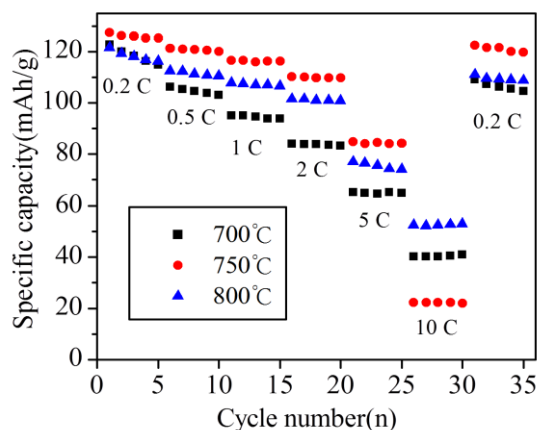


Figure 13. The rate profiles of the materials synthesized at 700 °C, 750 °C and 800 °C.

In order to prove more adequately that the synthesized sample has more excellent electrochemical performance, we made comparison with similar cathode materials for LIBs that were described in literature. The sample synthesized under the optimal conditions in this paper is labeled as S-1, S-2 and S-3 correspond to the samples synthesized in literature [31] and [2], respectively. Table 2 and 3 are the capacity comparison of several samples under different charge-discharge cycles and rates. From Table 2 we can see that, even at higher rates, the first discharge specific capacity of S-1 is similar to that of S-2. And the capacity retention ratio reached 87.3% after 100 charging cycles, which is higher than S-2 of 83.3%. The comparison with discharge capacity of different samples at different rates is shown in Table 3. Compared with S-2, Sample S-1 displays better discharge capacity at different rates. So, we can come to the conclusion, the sample S-1 exhibits superior electrochemical performances.

Table 2. The capacity comparison of several samples at different cycling number

Samples	Rate (C)	1 st Discharge Capacity (mAh·g ⁻¹)	100 th Discharge Capacity (mAh·g ⁻¹)	Capacity Retention Ratio
S-1	0.5	126	110	87.3
S-2	0.2	127.4	106.1	83.3

Table 3. The capacity comparison of several samples at different charge-discharge rates

Samples	Discharge capacity (mAh·g ⁻¹) at room temperature				
	0.2 C	1 C	2 C	5 C	0.2 C
S-1	128	118	116	84	126
S-3	124	116	112	99	123

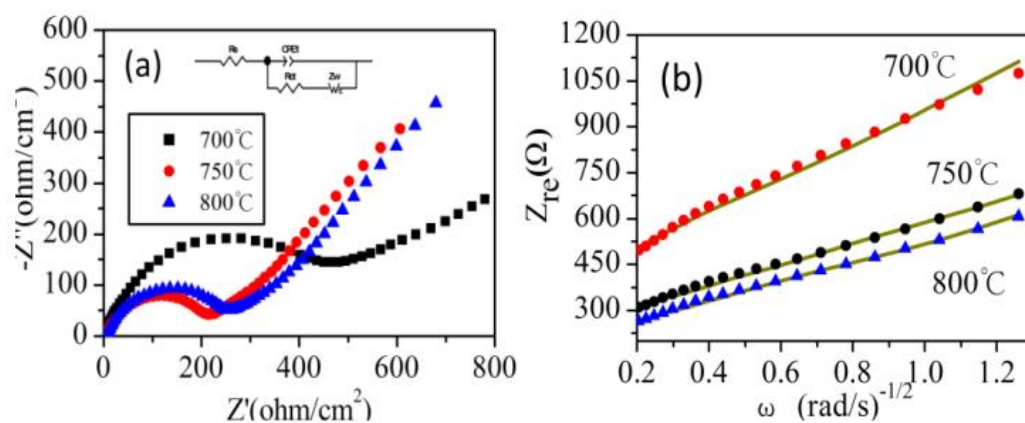


Figure 14. (a) The EIS of several materials synthesized at 700 °C, 750 °C and 800 °C, (b) AC impedance spectrum in low frequency region.

Based on the above analysis, we could conclude that the sample at 750 °C had best crystalline structure and no other impure phase, and smaller nanometer rod like spinel LiMn₂O₄ particles had a larger specific surface area, shortening the diffusion path of lithium ion in charge and discharge process as well as increasing the effective contact area between the material and the electrolyte. Thus compared with other samples, it had the best electrochemical performances.

Figure 14 (a) showed the electrochemical impedance spectra (EIS) of LiMn₂O₄ materials prepared at different sintering temperatures. As we all known, the high-frequency semicircle reacted to the charge transfer resistance (R_{ct}) which was caused by charge transfer across the electrode electrolyte interface, the diameter of semicircle was approximately equal to the charge transfer resistance (R_{ct}). The straight line of low frequency area presented Li⁺ diffusion resistance in electrode bulk, namely, the Warburg impedance (Z_w), which was associated with Li⁺ diffusion in lithium manganese particles [32-34]. By fitting data, the charge transfer impedance values of three samples sintered at 700 °C, 750 °C, 800 °C were 365 Ω, 197 Ω and 235 Ω, and the error values corresponded with 1.77%, 1.22%, 1.10%, respectively. The sample sintered at 750 °C had the lowest charge transfer impedance. The AC impedance spectrum of low frequency region was displayed in Figure 14 (a), a linear relationship of Z_{re} and ω^{-1/2} through data fitting was obtained, the slope of which was the Warburg coefficient, according to the following formula:

$$Z_{re} = R_{\Omega} + R_{ct} + \sigma \omega^{-1/2}$$

Z_{re} was the real part of the impedance, ω was angular frequency, σ was the Warburg coefficient. The lithium ion diffusion coefficient of the three samples at 700 °C, 750 °C and 800 °C were calculated separately 6.31×10^{-17} , 1.93×10^{-16} , 1.72×10^{-16} , which was believed to have a great relationship between particles size. The sample for 750 °C had a smallest particle size, as well as the shortest lithium ion diffusion path. Combined with the morphology and structure of the materials, it could be deduced that the sample sintered at 750 °C possessed better lithium ion insertion and extraction mechanism.

4. CONCLUSIONS

Optimized the reaction temperature and reaction time, MnO_2 precursors with a spiny spherical morphology, uniform dispersion and core-shell structure was synthesized by hydrothermal method. Then, using MnO_2 precursors as manganese source, $LiOH \cdot H_2O$ as lithium source, spinel $LiMn_2O_4$ cathode materials with excellent electrochemical performances was synthesized by high temperature solid phase method through optimizing the sintering temperature and other technological conditions.

Therefore, the structure and electrochemical properties of $LiMn_2O_4$ cathode materials can be effectively improved by choosing the proper synthesis methods and synthesis conditions. But in view of the special structure and properties of $LiMn_2O_4$ cathode materials, the selection of ideal coating materials and coating methods, as well as the synergistic doping of composite ions, will be a very important means to improve the rate capability and cycle performance of lithium manganese oxide cathode materials, which are what our team will do next.

ACKNOWLEDGEMENTS

This work was financially supported by the National Science Foundation of China (Grant No. 51364008) and the Science, Technology Research Projects of Guangxi institution of higher education (Grant No. 2013ZD030) and the Guangxi Natural Science Foundation (Grant No. 2014GXNSFAA118046).

References

1. Y. Cui, W. Bao, Z. Yuan, Q. Zhuang and Z. Sun, *J. Solid State Electrochem.*, 16 (2012) 1551.
2. D. Guo, Z. Chang, B. Li, H. Tang and X.Z. Yuan, *J. Solid State Electrochem.*, 17 (2013) 2849.
3. M.A. Kiani, M.F. Mousavi and M.S. Rahmanifar, *Int. J. Electrochem. Sci.*, 6 (2011) 2581.
4. S. Lee, Y. Cho, H. Song, K.T. Lee and J. Cho, *Angew. Chem., Int. Ed.*, 51 (2012) 8748.
5. L.J. Xi, H.E. Wang, Z.G. Lu, S.L. Yang, R.G. Ma and J.Q. Deng, C.Y. Chung, *J. Power Sources*, 198 (2012) 251.
6. J.Y. Luo, X.L. Li and Y.Y. Xia, *Electrochim. Acta*, 52 (2007) 4525.
7. H. Xia, Z. Luo and J. Xie, *Progress in Natural Science: Materials International*, 22 (2012) 572.
8. M.H. Bhat, B.P. Chakravarthy, P.A. Ramakrishnan, A. Levasseur and K.J. Rao, *Bull. Mater. Sci.*, 23 (2000) 461.
9. R. Wang, Z. Wang, X. Li and H. Zhang, *Electrochim. Acta*, 241 (2017) 208.
10. R. Wang, X.Li, Z. Wang and H. Zhang, *Nano Energy*, 34 (2017) 131.

11. A. Eftekhari, *Solid State Ionics*, 167 (2004) 237.
12. Y.L. Ding, J. Xie, G.S. Cao, T.J. Zhu, H.M. Yu and X.B. Zhao, *Adv. Funct. Mater.*, 21 (2011) 348.
13. W.S. Yoon, J. Hanson, J. Mcbreen and X.Q. Yang, *Electrochem. Commun.*, 8 (2006) 859.
14. T. Aoshima, K. Okahara, C. Kiyohara and K. Shizuka, *J. Power Sources*, 377 (2001) 97.
15. J. Jiang, K. Du, Y. Cao, Z. Peng, G. Hu and J. Duan, *J. Alloys Compd.*, 577 (2013) 138.
16. T.F. Yi, C.L. Hao, C.B. Yue, R.S. Zhu and J. Shu, *Synth. Met.*, 159 (2009) 1255.
17. J.W. Lee, J.I. Kim and S.H. Min, *J. Power Sources*, 196 (2011) 1488.
18. X.M. He, J.J. Li, Y. Cai, Y.W. Wang, J.R. Ying, C.Y. Jiang and C.R. Wan, *Key Engineering Materials*, 438 (2007) 336.
19. H. Yue, X. Huang, D. Lv and Y. Yang, *Synth. Met.*, 54 (2009) 5363.
20. Y.Z. Wang, X. Shao, H.Y. Xu, M. Xie, S.X. Deng, H. Wang, J.B. Liu and H. Yan, *J. Power Sources*, 226 (2013) 140.
21. G.E. Blomgren, *J. Electrochem. Soc.*, 164 (2017) A5019.
22. A. Yano, M. Shikano, A. Ueda, H. Sakaebe and Z. Ogumi, *Int. J. Electrochem. Sci.*, 164 (2017) A6116.
23. M.E. Spahr, P. Novak, B. Schnyder, O. Haas and R. Nesper, *Int. J. Electrochem. Sci.*, 145 (1998) 1113.
24. Y. Zhang, B. Wang, M. Nie, F. Yu, Y. F. Xia, B. S. Liu, Y. Xue, L. L. Zheng and J. Wu, *RSC Adv.*, 6 (2016) 70.
25. X. Wang and Y. Li, *J. Am. Chem. Soc.*, 124 (2002) 2880.
26. L. Noerochim, G. P. Sapputra and A. Widodo, *AIP Conference Proceedings*, 1725 (2016) 020054.
27. L. Feng, Z. Xuan, H. Zhao, Y. Bai, J. Guo and C. Su, *Nanoscale Research Letters*, 9 (2014) 290.
28. Q. Liu, K. Du and H. Guo, *Electrochim. Acta*, 90(2013) 350.
29. A. Yuan, L. Tian and W. Xu, *J. Power Sources*, 195(2010) 5032.
30. J. Y. Luo, Y. G. Wang, H. M. Xiong and Y. Y. Xia, *Cheminform.*, 38 (2007) 4791.
31. X. Lv, S. Chen, C. Chen, L. Liu, F. Liu and G. Qiu, *Solid State Sci.*, 31 (2014) 16.
32. R.K. Petla, B.N. Rao, P. Muralidharan, N. Satyanarayana and M. Venkateswarlu, *Int. J. Electrochem. Sci.*, 9 (2014) 1207.
33. Y.K. Sun and D.W. Kim, *Korean J. Chem. Eng.*, 16 (1999) 449.
34. M.A. Kiani, M.F. Mousavi and M.S. Rahmanifar, *Int. J. Electrochem. Sci.*, 6 (2011) 2581.

© 2018 The Authors. Published by ESG (www.electrochemsci.org). This article is an open access article distributed under the terms and conditions of the Creative Commons Attribution license (<http://creativecommons.org/licenses/by/4.0/>).